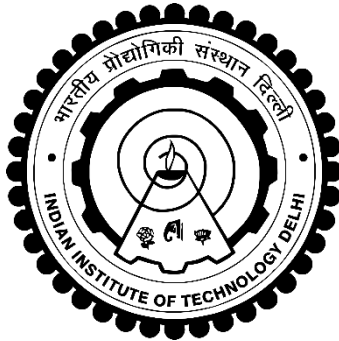


**NUMERICAL INVESTIGATION OF  
LIQUID–LIQUID DISENGAGEMENT IN A  
BATCH AND CONTINUOUS GRAVITY  
SETTLER**

**SAROJ KUMAR PANDA**



**DEPARTMENT OF CHEMICAL ENGINEERING  
INDIAN INSTITUTE OF TECHNOLOGY DELHI**

**OCTOBER 2018**

© Indian Institute of Technology Delhi (IITD), New Delhi, 2018

# NUMERICAL INVESTIGATION OF LIQUID–LIQUID DISENGAGEMENT IN A BATCH AND CONTINUOUS GRAVITY SETTLER

by

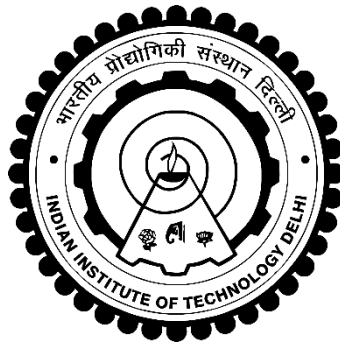
**SAROJ KUMAR PANDA**

Department of Chemical Engineering

Submitted

in fulfillment of the requirements of the degree of *Doctor of Philosophy*

to the



**INDIAN INSTITUTE OF TECHNOLOGY DELHI**

**OCTOBER 2018**

Dedicated to my beloved

*...Wife...*

## **Certificate**

This is to certify that the thesis entitled “**Numerical Investigation of Liquid–Liquid Disengagement in a Batch and Continuous Gravity Settler**” being submitted by **Mr. Saroj Kumar Panda** to the Indian Institute of Technology Delhi for the award of the degree of **Doctor of Philosophy** is a bonafide record of original research work carried out by him under my supervision in conformity with rules and regulations of the Institute. The results contained in this thesis have not been submitted elsewhere, either in part or in full, to any other University or Institute for the award of any degree or diploma.

Date:

**Dr. Vivek V. Buwa**

Professor

Department of Chemical Engineering,

Indian Institute of Technology Delhi,

New Delhi–110016, India.

## **Acknowledgements**

I consider myself very fortunate to become part of the Department of Chemical Engineering, IIT Delhi. The time spent here has enriched me academically and personally. It expanded my horizon. The legacy of the Institution encouraged me, inspired me to dream and work hard. I am indebted and will remain eternally so, to this Institution for providing me the facility to carry out my thesis work.

Every project begins with an idea and it completes with meticulous execution. I sincerely acknowledge my supervisor Prof. Vivek V. Buwa as the originator of this project. His meticulous plan and outstanding management have helped me in executing this work. I am grateful to him for choosing me as his student and giving an opportunity to work on this project. The work with him has improved me as a person and his rigorous scrutiny taught me to excel. I thank him for his readiness to correct my thesis, manuscripts and other internal reports with utmost priority despite his busy schedule. I sincerely appreciate his generosity, mentorship and mental support during this work.

I sincerely acknowledge the role of my Ph.D. committee members: Prof. Ratan Mohan, Prof. Paresh Chokshi and Prof. Amit Gupta for their critical review to improve the quality of the thesis work. The valuable suggestions were encouraging and stimulating.

I affectionately recollect my days with Abdul for being a friend, companion and a younger brother. His company was refreshing, stimulating and joyful. I not only acknowledge him for his warmth and care but also thank him for taking special care of my taste bud.

I genially acknowledge Abhijeet for being an integral part of my personal and professional life in IIT Delhi. It would not be possible to complete this work without his help. The long technical discussions with him were fortifying. I also owe him a lot for taking care of my health.

I truly acknowledge Brajesh as a right company during my coursework in the initial stage of Ph.D. and many important discussions at later stage as well. Any discussion with him really refreshing and satisfying. I deeply value the fond memories of the time spent with my present lab mates Ekta, Sirisha, Sayantani, Gaurav, Aniket, Karthik, Siddhartha, Swapnil, Shivam and my past lab mates Parul, Rajesh, Arpit, David, Raj Gopal and Prakhar.

I sincerely thank Anil for his unconditional help during my tenure in IIT Delhi. I warmheartedly reminisce the help of Raktika to manage stress and her care during several occasions of my hospitalization due to ill health. I thank Abhinav, Hari, Amit and others for making my hostel life in IIT Delhi cheerful. I fondly recognize the friendly staffs from hostel and mess for taking care of my special food and other requirements.

The financial support received for my project work from Bhabha Atomic Research Center (BARC), financial support received for my travels from IRD, IITD and support from FITT is greatly acknowledged. Particularly, I thank Dr. K. K. Singh, Mr. K. T. Shenoy, Mr. Nirvic Sen, and Mr. Mayur Darekar for their help during the experimental work and valuable discussions in BARC.

I would like to cordially acknowledge my friends Vaiju, Sanju and Nagaraja for taking care of Dipti in my absence. I especially thank Vaiju for providing me a shoulder to cry and being a sympathetic listener to me. I thank Nisha for giving me all kind of indulgence with my favorite foods during my visit to Kalpakkam. I thank Shri Utpal Borah, Aashranth, Santosh and Parthasarathi for their readiness to help me and their cordial interactions with me during my visits to IGCAR.

Everybody knows the ability to work for long hours, depends on your fitness. I owe a lot to both Dr. Mahesh Sagar and Dr. Rajlaxmi Borah for keeping me in a condition that permitted my long working hours during this work. Discussions during my sessions with them were great for both body and mind.

I would love to acknowledge the silent support provided by my Father-in-law and Mother-in-law for my Ph.D. work. They have been with me through thick and thin without any question.

The thesis work will remain incomplete without acknowledging my siblings. My younger sister has played a great role in my life by listening to my useless advice and in turn, by satisfying my big brother ego. Though being the youngest one in the family, my brother carried the burden of being the head of the house, during my thesis work. None of my words are good enough to acknowledge my brother's care of our single mother and managing all other social responsibilities in my long absence.

No words can describe the contribution of a mother in her child's work. Her wellbeing provides emotional stability and hope. I still acknowledge her for taking care of the house alone, taking care of her health and providing me the freedom to choose a career.

Finally and most importantly, I would like to thank my wife Dipti for her unconditional love and support. Her encouragement, patience and unwavering love were undeniably the bedrock upon which the past seventeen years of my life have been built. Her tolerance of my occasional arrogant moods is a testament in itself of her unyielding devotion and love. I thank her for the faith in me and allowing me to be as ambitious as I wanted. It was under her watchful eye that I gained so much drive and an ability to tackle challenges.

Above all, I thank the Almighty God for giving me the strength to bear the hardship during the difficult phases of my life.

**Saroj Kumar Panda**

## Abstract

The present research work is focused on the disengagement of liquid–liquid dispersion in a batch and continuous gravity settler using measurements and numerical simulations in OpenFOAM. Further, to developed an experimentally verified computational model that can predict the dynamics of such liquid–liquid flow in continuous and liquid phase disengagement in batch settler under different flow conditions (e.g. flow rate and fluid properties), internals (e.g. baffles, picket fence), different geometrical features (e.g. settler length, position of outlets, position of end–plate) and with different phase ratios.

Three–dimensional Eulerian–Eulerian (EE) simulations were performed by developing further the *twoPhaseEulerFoam* module of OpenFOAM. The effects of total liquid flow rate, drop diameter and organic phase density were investigated. The predicted effect of total liquid flow rate on dispersion–band thickness and organic phase volume fraction were compared with the measurements performed in a laboratory–scale continuous gravity settler. The drag coefficient correction factor was introduced in the drag model to account the drop swarms, led to improvements in the predictions of dispersion–band thickness and dispersed–phase volume fraction. The predicted results were found to be in a satisfactory agreement with the measurements. The observed difference in the measured and predicted results was due to the constant drop size considered in simulations.

The *twoPhaseEulerFoam* module was further used to perform EE simulations to study the effects of settler geometry (settling area, locations of aqueous phase outlet, position of end–plate) on the liquid–liquid separation in a continuous gravity settler. For a given flow rate of the dispersion, increase in the settler length (for a fixed width) led to increased settling area and also to increased residence time. It was found that, for settlers with  $L/W > 1.5$ , the insertion of picket fence did not improve the separation performance. However, for smaller  $L/W$ , the

insertion of picket fence led to a reduction in the dispersion–band thickness. The reduction in the aqueous outlet and end–plate height after certain level, no phase separation was achieved. A new correlation was developed for prediction of the dispersion–band thickness that successfully predicts the effects of dispersion flow rate, settling area, inlet baffle opening position, inlet phase ratio and the density ratio.

Further, the need of batch settling was studied by performing experiments in a laboratory–scale batch settler and later EE simulations were performed using the same geometry and dimension of the settler. The effects of organic (dispersed) to aqueous (continuous) phase ratio ( $\alpha_a/\alpha_b$ ), impeller speed and phase properties were studied in detail. The predicted and measured dispersion–band thickness (position of active and passive interface), organic (dispersed) phase volume fraction were compared and a satisfactory agreement was obtained. As expected, high impeller speed generates smaller drop size that led to a longer time for phase separation. For a fixed impeller speed, decreasing the  $\alpha_a/\alpha_b$  ratio reduces the separation time (case of varying initial dispersion height). However, the phase separation time is increased significantly when the  $\alpha_a/\alpha_b$  in a constant initial dispersion height system is decreased. It was observed that due to high interfacial tension, kerosene–water system took longer time for phase separation compared to dodecane–nitric acid system.

The multi–fluid EE simulations (with and without PBM) were performed in the batch settler. The integration of a stand–alone population balance (PBM) code in the OpenFOAM CFD solver was carried out. The CFD+PBM solver (*multiPhaseCfdPbmFoam*) was used to perform 3D/laminar simulations in a batch settler to see the predictive capability of the model. For this purpose, the predicted active/passive interface and organic phase volume fraction distribution are compared with the measured data. The present work will be useful for the design of an optimal continuous settler configuration.

## सार

वर्तमान शोध कार्य ओपनफोम में माप और संख्यात्मक सिमुलेशन का उपयोग करके एक बैच और निरंतर गुरुत्वाकर्षण निपटान में तरल-तरल फैलाव के विघटन पर केंद्रित है। इसके अलावा, एक प्रयोगात्मक रूप से सत्यापित कम्प्यूटेशनल मॉडल विकसित करने के लिए जो विभिन्न प्रवाह स्थितियों) जैसे प्रवाह दर और द्रव गुण (के तहत बैच सेटलर में निरंतर और तरल चरण विघटन में ऐसे तरल-तरल प्रवाह की गतिशीलता की भविष्यवाणी कर सकता है, आंतरिक) जैसे बफफलेस, पिकेट-फेंस (, विभिन्न ज्यामितीय विशेषताएं) जैसे सेटलर लेंथ, आउटलेट की स्थिति, अंत प्लेट की स्थिति (और विभिन्न चरण अनुपात के साथ।

ओपन फोम के *टूफेजयूलरफोम* मॉड्यूल से त्रि-आयामी यूलरियन-यूलरियन ( ईई )सिमुलेशन किया गया तत्पश्चात कुल तरल प्रवाह दर, ड्रॉप व्यास और कार्बनिक चरण घनत्व के प्रभाव की जांच की गई। फैलाव-बैंड मोटाई और कार्बनिक चरण मात्रा अंश पर कुल तरल प्रवाह दर का अनुमानित प्रभाव एक प्रयोगशाला-पैमाने के निरंतर गुरुत्वाकर्षण निपटान में किए गए माप के साथ तुलना की गई। ड्रैग गुणांक सुधार कारक ड्रैग मॉडल में ड्रॉप स्वार्म्स को ध्यान में रखकर पेश किया गया था, जिससे डिस्पेरशन- बैंड मोटाई और डिस्पेर्सेड फेज वाले चरण मात्रा अंश की भविष्यवाणियों में सुधार हुआ और नतीजतन अनुमानित परिणाम माप के साथ संतोषजनक समझौते में पाए गए थे। मापा और अनुमानित परिणामों में पाए गए अंतर अनुकरण में निरंतर ड्रॉप आकार के कारण था।

तत्पश्चात *टूफेजयूलरफोम* मॉड्यूल का उपयोग निरंतर गुरुत्वाकर्षण निपटान में तरल-तरल पृथक्करण पर बसने वाले ज्यामिति (सेटलिंग एरिया, जलीय चरण आउटलेट के स्थान, अंत प्लेट की स्थिति) के प्रभावों का अध्ययन करने के लिए ईई सिमुलेशन करने के लिए किया गया । डिस्पेरशन की दी गई प्रवाह दर के लिए, बसने की लंबाई) एक निश्चित चौड़ाई के लिए (में वृद्धि के कारण निपटारे क्षेत्र में वृद्धि हुई और निवास के समय में वृद्धि हुई। यह पाया गया कि, एल / डब्ल्यू > 1 . 5के साथ बसने वालों के लिए, पिकेट-फेंस के सम्मिलन में पृथक्करण प्रदर्शन में सुधार नहीं हुआ। हालांकि, छोटे एल / डब्ल्यू के लिए, पिकेट-फेंस के सम्मिलन ने डिस्पेरशन- बैंड मोटाई में कमी आई।

कुछ स्तर के बाद जलीय आउटलेट और अंत-प्लेट ऊंचाई में कमी, कोई चरण अलगाव हासिल नहीं किया गया। डिस्पेरशन- बैंड मोटाई की भविष्यवाणी के लिए एक नया सहसंबंध विकसित किया गया था जो डिस्पेरशन प्रवाह दर, क्षेत्र को व्यवस्थित करने, इनलेट बापफ खोलने की स्थिति, इनलेट चरण अनुपात और घनत्व अनुपात के प्रभावों की सफलतापूर्वक भविष्यवाणी करता है। इसके अलावा, बैच निपटारे की आवश्यकता का प्रयोग प्रयोगशाला-स्केल बैच बसने

में प्रयोग करके किया गया था और बाद में ईई सिमुलेशन उसी ज्यामिति और बसने वाले के आयाम का उपयोग करके किया गया था। जलीय) निरंतर (चरण अनुपात)  $\alpha_a / \alpha_b$ ), प्ररित करनेवाला गति और चरण गुणों के लिए कार्बनिक) डिस्पेर्सिड (का प्रभाव विस्तार से अध्ययन किया गया था। अनुमानित और मापा फैलाव-बैंड मोटाई) सक्रिय और निष्क्रिय इंटरफेस की स्थिति(, कार्बनिक) डिस्पेर्सिड (चरण मात्रा अंश की तुलना की गई और एक संतोषजनक समझौता प्राप्त किया गया। जैसा कि अपेक्षित था, उच्च प्रवेगक गति छोटे ड्रॉप आकार उत्पन्न करती है जिससे चरण अलग होने के लिए लंबा समय लगता है। एक निश्चित प्ररित करनेवाला गति के लिए,  $\alpha_a / \alpha_b$  अनुपात घटाने से पृथक्करण समय कम हो जाता है । हालांकि, चरण पृथक्करण समय में काफी वृद्धि हुई है जब निरंतर प्रारंभिक डिस्पेरशन ऊंचाई प्रणाली में  $\alpha_a / \alpha_b$  में कमी आई है। यह देखा गया था कि उच्च इंटरफेसियल तनाव के कारण, केरोसिन-जल प्रणाली में डोडकेन-नाइट्रिक एसिड प्रणाली की तुलना में चरण पृथक्करण के लिए अधिक समय लगा।

बैच बसने वाले में बहु-द्रव ईई सिमुलेशन( पीबीएम के साथ और बिना) (किए गए थे। ओपनएफएएम सीएफडी सॉल्वर में स्टैंड-अलोन आबादी बैलेंस) पीबीएम (कोड का एकीकरण किया गया था। सीएफडी + पीबीएम सॉल्वर) *मल्टीफेस सीएफडीपीबीएमएफओएम* (मॉडल की भविष्यवाणी क्षमता देखने के लिए बैच बसने वाले में 3 डी / लैमिनार सिमुलेशन करने के लिए प्रयोग किया जाता था। इस उद्देश्य के लिए, अनुमानित सक्रिय / निष्क्रिय इंटरफेस और कार्बनिक चरण मात्रा अंश वितरण मापा डेटा के साथ तुलना की जाती है। वर्तमान कार्य एक इष्टतम निरंतर निपटान विन्यास के डिजाइन के लिए उपयोगी होगा।

# Table of Contents

<b>Certificate.....</b>	<b>i</b>
<b>Acknowledgements.....</b>	<b>ii</b>
<b>Abstract.....</b>	<b>v</b>
<b>Table of Contents .....</b>	<b>vii</b>
<b>List of Figures.....</b>	<b>xii</b>
<b>List of Tables.....</b>	<b>xx</b>
<b>Nomenclature.....</b>	<b>xxi</b>
<b>Chapter 1: Introduction .....</b>	<b>1</b>
1.1 Overview of solvent extraction process .....	2
1.2 Present state of art .....	8
1.2.1 Liquid–liquid disengagement in extraction equipment.....	8
1.2.2 Liquid–liquid disengagement in batch settlers.....	9
1.2.3 Liquid–liquid flow in continuous settlers .....	11
1.2.4 Population balance modeling in multiphase systems.....	14
1.3 Motivation of the present work .....	16
1.4 Specific objectives .....	17
1.5 Organization of thesis .....	18
<b>Chapter 2: Computational Model and Solution Methodology.....</b>	<b>21</b>
2.1 Computational model.....	22
2.2 Problem statement and solution methodology.....	23

2.3	OpenFOAM .....	24
2.3.1	Case structure in OpenFOAM.....	25
2.4	Implementation of two–fluid and multi–fluid Eulerian model in OpenFOAM .....	26
2.4.1	Two–/multi–fluid governing equations.....	27
2.4.1.1	<i>Mass and momentum conservation equations</i> .....	27
2.4.1.2	<i>Drag model</i> .....	28
2.4.1.3	<i>Lift model</i> .....	29
2.4.1.4	<i>Turbulence model</i> .....	30
2.4.2	Two–/multi–fluid model implementation in OpenFOAM.....	31
2.4.2.1	<i>Two–fluid model implementation</i> .....	31
2.4.2.2	<i>Multi–fluid model implementation</i> .....	33
2.5	Boundary conditions and numeric .....	34
2.6	Verification of two–fluid and multi–fluid model with measurements .....	37
2.6.1	Effect of superficial gas velocity on time–averaged gas volume fraction and vertical liquid velocity .....	37
2.7	Summary and conclusions .....	43

**Chapter 3: Simulations of Liquid–Liquid Disengagement in a Continuous Gravity Settler and Experimental Verification ..... 44**

3.1	Experiments on continuous gravity settler .....	45
3.2	Problem statement and solution methodology.....	46
3.3	Governing equations.....	49
3.4	Boundary conditions and discretization schemes.....	51

3.5	Preliminary simulations and effect of grid resolution .....	53
3.6	Effect of total flow rate on dispersion–band thickness and experimental verification .....	57
3.7	Comparison of predicted and measured dispersed–phase volume fraction....	62
3.8	Effect of drag corrections .....	63
3.9	Effect of inlet drop size on dispersion–band thickness .....	66
3.10	Effect of organic phase density on phase separation .....	72
3.11	Summary and conclusions .....	73

**Chapter 4: Optimization of Geometry and Internals of Continuous Gravity Settler for Liquid–Liquid Separation ..... 75**

4.1	Introduction.....	76
4.2	Comparison of predicted and measured dispersion–band thickness and organic phase volume fraction.....	78
4.3	Effect of settler length on phase separation.....	81
4.4	Arrangement of inlet baffle, dispersion–band thickness and separation performance .....	86
4.5	Effect of picket fence on separation performance .....	89
4.6	Effect of end–plate height and aqueous phase outlet position on phase separation .....	99
4.7	Effect of inlet volume fraction.....	103
4.8	Correlation for prediction of dispersion–band thickness.....	105
4.9	Summary and conclusions .....	108

**Chapter 5: Experimental Investigations on Liquid–Liquid Disengagement  
in a Batch Settler..... 110**

5.1 Introduction..... 111

    5.1.1 Motivation of the present investigations ..... 111

5.2 Experimental set–up and procedure ..... 112

5.3 Phase separation characteristics..... 116

5.4 Effect of organic to aqueous ( $\alpha_a/\alpha_b$ ) ratio ..... 117

    5.4.1 Positions of active and passive interfaces ..... 117

    5.4.2 Organic phase volume fraction ..... 121

5.5 Effect of phase properties on separation performance ..... 124

5.6 Summary and conclusions ..... 129

**Chapter 6: Two–Fluid Simulations of Liquid–Liquid Disengagement in a  
Batch Settler and Experimental Verification..... 130**

6.1 Problem statement and solution methodology..... 131

6.2 Governing equations..... 132

6.3 Boundary conditions and numeric ..... 132

6.4 Preliminary simulations and effect of grid resolution ..... 133

6.5 Comparison of predicted and measured position of active and passive interface  
..... 136

6.6 Comparison of predicted and measured organic phase volume fraction with  
different  $\alpha_a/\alpha_b$ ..... 139

6.7	Effect of drag correction on position of active/passive interface and organic phase volume fraction.....	142
6.8	Conclusions from two-fluid simulations in comparison with the measurements .....	145
6.9	Population balance for multiphase systems.....	146
6.10	Multi-fluid simulations in batch settler without PBM model .....	148
6.11	Integration of population balance model in CFD model .....	152
6.11.1	Multi-fluid model with source/sink .....	154
6.11.2	Formulation of drop Population Balance Equation (PBE).....	155
6.11.2.1	<i>Binary and interfacial coalescence kernels</i> .....	157
6.11.3	Method of Classes (CM) solution scheme .....	158
6.12	Multi-fluid simulations in batch settler with PBM model .....	160
6.12.1	Simulated positions of AI and PI and organic phase volume fraction with binary coalescence compared with the measurements .....	161
6.12.2	Comparison of position of AI and PI with binary and interfacial coalescence .....	165
<b>Chapter 7: Summary, Conclusions and Suggestions for Future Work.....</b>		<b>169</b>
7.1	Summary and conclusions .....	170
7.2	Suggestions for the future work.....	176
<b>References.....</b>		<b>177</b>
<b>List of Publications.....</b>		<b>185</b>
<b>Bio-Data.....</b>		<b>187</b>

## List of Figures

Figure 1.1. Basic principle of PUREX process.....	3
Figure 1.2. Equipment for liquid–liquid extraction (a) pulsed column, (b) centrifugal contactor, (c) mixer–settler. (Source: Simpson (2013) and Wardle et al. (2008)). .....	4
Figure 1.3. Schematic of liquid–liquid extraction process using mixer–settler.....	5
Figure 2.1. Schematic representation of (a) geometry of the rectangular bubble column and (b) computational grid. ....	24
Figure 2.2. Overview of OpenFOAM structure.....	25
Figure 2.3. Typical case structure in OpenFOAM.....	26
Figure 2.4. Comparison of predictions of two–fluid (constant $C_D$ and $C_L$ ) and multi–fluid models (size dependent $C_D$ and $C_L$ ) (a) time–averaged gas hold–up profiles and (b) time–averaged vertical liquid velocity, at superficial gas velocity 0.14 cm/s ( $H/W = 2.25$ , $Y = 37$ cm).....	39
Figure 2.5. Comparison of predictions of two–fluid and multi–fluid models for time–averaged gas hold–up at superficial gas velocity 0.73 cm/s ( $H/W = 2.25$ , $Y = 37$ cm). ....	40
Figure 2.6. Computational snapshots of oscillating bubble plume (gas hold–up distribution) for different bubble diameter at superficial gas velocity of 0.73 cm/s ( $H/W = 2.25$ ) .....	40
Figure 2.7. Time–averaged gas volume fraction distribution profiles at superficial gas velocity 0.73 cm/s for size dependent $C_D$ and $C_L$ multi–fluid calculations ( $H/W = 2.25$ , $Y = 37$ cm)..	41

Figure 2.8. Comparison of two–fluid and multi–fluid simulations of horizontal liquid velocity at $x = 0.1$ m along the width of the column at superficial velocity $0.73$ cm/s ( $Y = 25$ cm from the bottom).....	41
Figure 2.9. Effect of superficial gas velocity on plume oscillation period.....	42
Figure 3.1. Typical laboratory scale mixer–settler (1: Impeller, 2: Mixer, 3: Feed tank, 4: Settler, 5: Organic outlet, 6: Aqueous outlet, 7: Vertical slots, 8: Sample withdrawal ports)....	45
Figure 3.2. (a) Schematic of the settler with dimensions, (b) inlet baffle and (c) picket fence (all dimensions are in <i>mm</i> ).....	47
Figure 3.3. (a) Boundary conditions and different parts of the settler (1: Inlet, 2: Baffle, 3: Picket fence, 4: Bottom surface, 5: End-plate, 6: Guide-plate, 7: Top surface, 8: Organic outlet, 9: Aqueous outlet) and (b) schematic of the computational mesh used in the present work.....	48
Figure 3.4. Snapshot of simulated organic phase volume fraction distribution in a continuous gravity settler. ....	53
Figure 3.5. Snapshots showing the simulated time evolution of organic phase volume fraction and dispersion–band thickness at (a) 60 s, (b) 100 s, (c) 140 s, (d) 180 s, (e) 220 s and.....	54
Figure 3.6. (a) Simulated time evolution of position of AI and PI along the length of the settler for medium grid and (b) effect of grid resolution on position of AI and PI along the length of the settler ( $L = L_{ref}$ ) at steady state for different grids ( <i>AI: Active interface, PI: Passive interface</i> ) ( $t = 250$ s, $Q_t = 400$ l/hr, $d_d = 100$ $\mu$ m).....	56

Figure 3.7. Effect of total liquid flow rate on organic phase volume fraction distribution and dispersion–band (a) 200 l/hr, (b) 300 l/hr, (c) 400 l/hr, (d) 600 l/hr, (e) 800 l/hr and (f) 1000 l/hr (at $t = 250$ s, $d_d = 100$ $\mu\text{m}$ ).....	57
Figure 3.8. Effect of total liquid flow rate on organic phase flow field at different flow rates (a) 200 l/hr, (b) 300 l/hr, (c) 400 l/hr, (d) 600 l/hr, (e) 800 l/hr and (f) 1000 l/hr (at $t = 250$ s, $d_d = 100$ $\mu\text{m}$ ).....	58
Figure 3.9. Comparison of predicted and measured dispersion–band thickness at $Q_t = 400$ l/hr ( $d_d = 129$ $\mu\text{m}$ ) and 800 l/hr ( $d_d = 148$ $\mu\text{m}$ ) and (b) dispersion–band thickness versus specific settling rate of dispersed–phase at steady state ( $t = 250$ s). ....	61
Figure 3.10. Comparison of predicted steady state organic phase volume fraction with the measurements at $Q_t$ of (a) 400 l/hr ( $d_d = 129$ $\mu\text{m}$ ) and (b) 800 l/hr ( $d_d = 148$ $\mu\text{m}$ ).....	63
Figure 3.11. Comparison of measured and predicted (a) dispersion–band thickness and (b) organic phase volume fraction using no drag correction and drag correction of 0.1, 0.5 and 1 at $Q_t$ of 800 l/hr ( $d_d = 129$ $\mu\text{m}$ , $\alpha_{o,inlet} = \alpha_{a,inlet} = 0.5$ , $L = L_{ref}$ ); Symbols and lines indicate experimental and simulated results, respectively ( <i>NC: No drag correction, WC: With drag correction</i> ).....	65
Figure 3.12. Effect of drop size on dispersion–band thickness (i) 100 $\mu\text{m}$ , (ii) 200 $\mu\text{m}$ and (iii) 1000 $\mu\text{m}$ (a) organic phase.....	68
Figure 3.13. Effect of flow rate on the structure of dispersion–band thickness (i) 600 l/hr, (ii) 800 l/hr and (iii) 1000 l/hr (a) organic .....	69
Figure 3.14. Effect of (a) $d_d$ at $Q_t = 400$ l/hr and (b) $Q_t$ at $d_d = 200$ $\mu\text{m}$ on organic phase volume fraction fluctuations ( $t = 250$ s).....	70

Figure 3.15. Effect of organic phase density on dispersion–band thickness (a) 600 kg/m <sup>3</sup> , (b) 800 kg/m <sup>3</sup> , (c) 1000 kg/m <sup>3</sup> , (d) 1200 kg/m <sup>3</sup> ( $Q_t = 400$ l/hr, $d_d = 100$ μm).....	72
Figure 4.1. Effect of grid resolution on position of AI and PI along the length of the settler ( $L = 2L_{ref}$ ) at steady state ( <i>AI: Active interface, PI: Passive interface</i> ) ( $Q_d = 200$ l/hr, $d_d = 100$ μm). .....	77
Figure 4.2. Comparison of measured (Thaker et al., 2017) and predicted dispersion–band thickness at $Q_t$ of 600 l/hr ( $d_d = 138$ μm, $\alpha_{o,inlet} = \alpha_{a,inlet} = 0.5$ ) at different positions of end–plate (a) $L = L_{ref}$ , (b) $L = 0.67L_{ref}$ and (c) $L = 0.56L_{ref}$ along the length of the settler. ....	79
Figure 4.3. Comparison of predicted organic phase volume fraction with the measurements of Thaker et al., (2017) at $Q_t$ of 600 l/hr ( $d_d = 138$ μm, $\alpha_{o,inlet} = \alpha_{a,inlet} = 0.5$ ) at different position of end–plate (a) $L = L_{ref}$ , (b) $L = 0.67L_{ref}$ and (c) $L = 0.56L_{ref}$ . ....	81
Figure 4.4. Predicted steady state organic phase volume fraction distribution for settler lengths of (a) 59 cm ( $L_{ref}$ ), (b) 88.5 cm ( $1.5L_{ref}$ ) and (c) 118 cm ( $2L_{ref}$ ) ( $Q_t = 400$ l/hr, $\alpha_{o,inlet} = \alpha_{a,inlet} = 0.5$ , $d_d = 100$ μm). ....	82
Figure 4.5. Effect of settler length on steady state dispersion–band thickness for settler lengths of (a) 59 cm ( $L_{ref}$ ), (b) 88.5 cm ( $1.5L_{ref}$ ) and (c) 118 cm ( $2L_{ref}$ ) ( $Q_t = 400$ l/hr, $\alpha_{o,inlet} = \alpha_{a,inlet} = 0.5$ , $d_d = 100$ μm). ....	83
Figure 4.6. Effect of flow rate and settler length on residence time ( $\alpha_{o,inlet} = \alpha_{a,inlet} = 0.5$ , $d_d = 100$ μm). ....	83
Figure 4.7. Predicted steady state organic phase volume fraction distribution for $Q_t$ of 600 l/hr at (a) $L = L_{ref}$ , (b) $L = 1.5L_{ref}$ and (c) $L = 2L_{ref}$ ( $\alpha_{o,inlet} = \alpha_{a,inlet} = 0.5$ , $d_d = 100$ μm). ....	85

Figure 4.8. Schematic representation of inlet baffle (a) position 1 (18 cm), (b) position 2 (10 cm), (c) position 3 (2 cm) (all positions are from bottom of the settler) .....	85
Figure 4.9. Effect of inlet baffle position on dispersion–band for different position of baffle (a) position 1, (b) position 2 and (c) position 3 ( $t = 250$ s, $Q_t = 400$ l/hr, $d_d = 100$ $\mu$ m).....	87
Figure 4.10. Different arrangements of baffle and picket fence inside the settler (a) without picket fence, (b) picket fence at 2 <sup>nd</sup> slot, (c) picket fence at 4 <sup>th</sup> slot and (d) picket fence at 6 <sup>th</sup> slot.....	92
Figure 4.11. Effect of picket fence position on the simulated time evolution of organic phase volume fraction and dispersion–band thickness (a) 2 <sup>nd</sup> slot, (ii) 4 <sup>th</sup> slot and (iii) 6 <sup>th</sup> slot ( $Q_t = 400$ l/hr, $L = L_{ref}$ , baffle position: 1 <sup>st</sup> slot).....	93
Figure 4.12. Effect of picket fence position on dispersion–band thickness ( $Q_t = 400$ l/hr, $\alpha_{o,inlet} = \alpha_{a,inlet} = 0.5$ , $d_d = 100$ $\mu$ m, $L = L_{ref}$ , baffle position: 1 <sup>st</sup> slot). .....	94
Figure 4.13. Effect of picket fence (a) without picket fence and (b) with picket fence on the simulated time evolution of organic–aqueous phases separation and dispersion–band thickness at (i) 60 s, (ii) 180 s and (iii) 250 s ( $Q_t = 400$ l/hr, $\alpha_{o,inlet} = \alpha_{a,inlet} = 0.5$ , $d_d = 100$ $\mu$ m, $L = 0.75L_{ref}$ , $W = 0.334$ m). .....	95
Figure 4.14. Velocity vector field (a) without picket fence and (b) with picket fence on the simulated organic–aqueous phases separation ( $Q_t = 400$ l/hr, $L = 0.75L_{ref}$ ).....	96
Figure 4.15. Effect of picket fence for $d_d = 200$ $\mu$ m (a) without picket fence and with picket fence in (b) 2 <sup>nd</sup> slot, (c) 4 <sup>th</sup> slot and (d) 2 <sup>nd</sup> & 5 <sup>th</sup> slots on (i) phase separation and (ii) organic phase iso–surface ( $Q_t = 400$ l/hr, $L = L_{ref}$ ). .....	97

Figure 4.16. Comparison of organic phase volume fraction fluctuation time series along the length of the settler for (a) no picket fence and with picket fence in (b) 2 <sup>nd</sup> slot (c) 4 <sup>th</sup> slot and (d) 2 <sup>nd</sup> & 5 <sup>th</sup> slots ( $d_d = 200 \mu\text{m}$ , $Q_t = 400 \text{ l/hr}$ ) ( <i>PF: Picket fence</i> ). .....	98
Figure 4.17. Effect of end-plate height (a) 0.25 m, (b) 0.23 m and (c) 0.21 m from bottom on instantaneous organic phase volume fraction distribution ( $Q_t = 400 \text{ l/hr}$ , $L = 1.5L_{\text{ref}}$ , $\alpha_{o,\text{inlet}} = \alpha_{a,\text{inlet}} = 0.5$ , $d_d = 100 \mu\text{m}$ ). .....	102
Figure 4.18. Effect of aqueous phase outlet on the separation of organic and aqueous phases and dispersion-band thickness at $Q_t = 400 \text{ l/hr}$ (a) 0.23 m (b) 0.2 m, (c) 0.189 m and (d) 0.167 m (distances are from bottom of the settler) ( $L = L_{\text{ref}}$ , $\alpha_{o,\text{inlet}} = \alpha_{a,\text{inlet}} = 0.5$ , $d_d = 100 \mu\text{m}$ )....	103
Figure 4.19. Computational snapshots showing the separation of organic-aqueous phases and dispersion-band thickness at organic to aqueous ratio ( $\alpha_{o,\text{inlet}}:\alpha_{a,\text{inlet}}$ ) of (a) 0.5:0.5 (b) 0.4:0.6 and (c) 0.2:0.8 ( $Q_t = 400 \text{ l/hr}$ , $L = L_{\text{ref}}$ , $d_d = 100 \mu\text{m}$ ).....	104
Figure 4.20. Effect of $\alpha_{a,\text{inlet}}:\alpha_{b,\text{inlet}}$ on dispersion-band thickness ( $Q_t = 400 \text{ l/hr}$ , $L = L_{\text{ref}}$ , $d_d = 100 \mu\text{m}$ ).....	105
Figure 4.21. Variation of dispersion-band thickness with varying (a) baffle opening, (b) organic phase density, (c) specific settling area and (d) organic to aqueous phase ratio at inlet (simulated results versus prediction from Eq. 4.4). .....	106
Figure 4.22. Comparison of simulated and predicted (Eq. 4.4) values of dispersion-band thickness.....	107
Figure 5.1. (a) Typical laboratory-scale batch settler (1: Stirrer, 2: Impeller rod, 3: Settler vessel, 4: Baffles, 5: Impeller blade, 6: Sample withdrawal port, 7: Impeller speed controller	

and 8: Tachometer), (b) dimensions of settler vessel, (c & d) baffle and (e) impeller blade ( <i>all dimensions are in m</i> ).....	113
Figure 5.2. Schematic representation of (a) height of sedimentation and dense-packed zone and (b) position of Sedimenting and coalescing interface (Redrawn from <a href="#">Jeelani and Hartland (1998)</a> ).....	115
Figure 5.3. Schematic and dimensions of the different initial dispersion heights used to investigate the effects of $\alpha_a/\alpha_b$ in the settler (kerosene-water system) (all dimensions are in m).....	117
Figure 5.4. Variation in the positions of active and passive interfaces with time for different $\alpha_a/\alpha_b$ for impeller speeds of (a) 180, (b) 220 and (c) 260 rpm (kerosene-water system)....	120
Figure 5.5. Effect of $\alpha_a/\alpha_b$ on the organic phase volume fraction distribution: $\alpha_a/\alpha_b$ of (a) 1, (b) 0.84 and (c) 0.67 at impeller speeds of (i) 180, (ii) 220 and (iii) 260 rpm (kerosene-water system).....	123
Figure 5.6. Variation in the position of active and passive interface with time for different $\alpha_a/\alpha_b$ (a) 1, (b) 0.84 and (c) 0.67 (dodecane-nitric acid system). ....	126
Figure 5.7. Comparison of positions of AI and PI for KW and DN system at constant impeller speed of 220 rpm for different $\alpha_a/\alpha_b$ of (a) 1, (b) 0.84 and (c) 0.67 (KW: Kerosene-water and DN: Dodecane-nitric acid). ....	127
Figure 5.8. Comparison of organic phase volume fraction for KW and DN system at constant impeller speed of 220 rpm for different $\alpha_a/\alpha_b$ (a) 1, (b) 0.84 and (c) 0.67 (KW: Kerosene-water and DN: Dodecane-nitric acid).....	128

Figure 6.1. Schematic representation of (a) geometry and (b) computational mesh of the batch settler.....	131
Figure 6.2. Schematic representation of (a) geometry of the batch settler and (b) computational mesh.....	134
Figure 6.3. Effect of grid resolution on position AI and PI in batch settler at 260 rpm ( <i>AI: Active interface, PI: Passive interface</i> ) ( $\alpha_a/\alpha_b = 1$ , $d_d = 170 \mu\text{m}$ ).....	134
Figure 6.4. Comparison of (a) measured and (b) predicted time evolution of dispersion–band thickness for constant drop size ( $d_d$ ) of $198 \mu\text{m}$ at $\alpha_a/\alpha_b$ of 1. ....	135
Figure 6.5. Comparison of predicted (line) and measured (symbol) position of AI and PI at $\alpha_a/\alpha_b$ of (i) 1, (ii) 0.84 and (iii) 0.67 and at impeller speed of (a) 180 rpm, (b) 220 rpm and (c) 260 rpm ( <i>AI: Active interface, PI: Passive interface</i> ).....	138
Figure 6.6. Comparison of predicted (line) and measured (symbol) organic phase volume fraction at $\alpha_a/\alpha_b$ of (i) 1, (ii) 0.84 and (iii) 0.67 and at impeller speed of (a) 180 rpm, (b) 220 rpm and (c) 260 rpm. ....	141
Figure 6.7. Comparison of measured and predicted dispersion–band thickness using no drag correction and drag correction of 0.1 and 0.3 at $\alpha_a/\alpha_b$ of 1 and 220 rpm impeller speed ( $d_a = 200 \mu\text{m}$ ) ( <i>NC: No drag correction, WC: With drag correction</i> ). ....	143
Figure 6.8. Comparison of measured and predicted organic phase volume fraction using no drag correction and drag correction of 0.1, 0.3 and 0.5 at $\alpha_a/\alpha_b$ of 1 and 220 rpm impeller speed ( $d_a = 200 \mu\text{m}$ ) ( <i>NC: No drag correction, WC: With drag correction</i> ).....	144

Figure 6.9. Schematic representation of (a) two–fluid, (b) multi–fluid and (c) multi–fluid with PBM modeling.....	147
Figure 6.10. Schematic representation of (a) drop–drop coalescence, (b) breakage and (c) interfacial coalescence. ....	148
Figure 6.11. Simulated time evolution of aqueous phase volume fraction distribution at impeller speed of 220 rpm at $\alpha_a/\alpha_b$ of 1 (kerosene–water system).....	149
Figure 6.12. Simulated time evolution of organic phase volume fraction distribution of different drop size groups (a) 73 $\mu\text{m}$ , (b) 94 $\mu\text{m}$ , (c) 123 $\mu\text{m}$ , (d) 165 $\mu\text{m}$ and (e) 298 $\mu\text{m}$ (impeller speed = 220 rpm, $\alpha_a/\alpha_b = 1$ , kerosene–water system).....	151
Figure 6.13. Representation of Population Balance Model (PBM) integrated with CFD model. ....	153
Figure 6.14. Drop population describe by multi–group model (Redrawn from <a href="#">Buwa and Ranade (2002)</a> ).....	159
Figure 6.15. Simulated time evolution of (a) aqueous phase volume fraction distribution and (b) velocity vector with binary coalescence (impeller speed = 220 rpm, $\alpha_a/\alpha_b = 1$ , kerosene–water system). ....	163
Figure 6.16. Comparison of predicted two-fluid active and passive interfaces with measurements and predictions using multi-fluid + binary coalescence module (impeller speed = 220 rpm, $\alpha_a/\alpha_b = 1$ ( <i>BC: Binary coalescence</i> )).....	164

Figure 6.17. Comparison of predicted two-fluid organic phase volume fraction distribution with measurements and predictions using multi-fluid + binary coalescence module (impeller speed = 220 rpm,  $\alpha_a/\alpha_b = 1$  (*BC: Binary coalescence*))..... 164

Figure 6.18. Simulated time evolution of (a) aqueous phase volume fraction distribution and (b) velocity vector with binary + interfacial coalescence (impeller speed = 220 rpm,  $\alpha_a/\alpha_b = 1$ , kerosene–water system)..... 167

Figure 6.19. Comparison of simulated aqueous phase volume fraction distribution and corresponding velocity vector with (a) binary coalescence and (b) binary + interfacial coalescence (impeller speed = 220 rpm,  $\alpha_a/\alpha_b = 1$ , kerosene–water system)..... 168

Figure 6.20. Comparison of predicted active and passive interfaces from multi-fluid + BC and multi-fluid + IC modules with measurements for KW system (impeller speed = 220 rpm,  $\alpha_a/\alpha_b = 1$  (*BC: Binary coalescence, IC: Interfacial coalescence*))..... 168

## List of Tables

Table 2.1. Boundary conditions for the simulations of gas–liquid flows in bubble column ...	36
Table 2.2. Discretization schemes used in the present work .....	36
Table 3.1. Boundary conditions .....	52
Table 3.2. Discretization schemes used in the present work .....	52
Table 3.3. Variation of flow rate at outlets .....	60
Table 4.1. Effect of the dispersion entrance level (baffle opening position) .....	88
Table 4.2. Effect of end–plate height on separation performance .....	100
Table 4.3. Effect of aqueous outlet position on the separation performance .....	100
Table 5.1. Properties of the fluid phases used in the present work .....	114
Table 6.1. Boundary conditions .....	133

# Nomenclature

## Symbols

$A$	Settling area, $m^2$
$A_{CS}$	Cross-sectional area of the settler, $m^2$
$b(v)$	Breakage frequency, $s^{-1}$
$B_c$	Birth term due to coalescence, $m^3/s$
$B_b$	Birth term due to breakage, $m^3/s$
$C_1, C_2$	Model parameters in turbulence model, (-)
$C_1-C_{23}$	Adjustable parameters, (-)
$C'_1-C'_{24}$	Adjustable parameters, (-)
$C_D$	Drag coefficient, (-)
$C_L$	Lift coefficient, (-)
$C_{VM}$	Virtual mass coefficient, (-)
$d_B$	Bubble diameter, m
$d_d$	Diameter of drop, $\mu m$
$D_c$	Death term due to coalescence, $m^3/s$
$D_b$	Death term due to breakage, $m^3/s$
$E\ddot{o}$	Eotvos number, (-)
$f(x, t)$	Particle number distribution, (-)
$F$	Force, N
$G, G_e$	Turbulence generation, extra source of turbulence due to dispersed phase
$g$	Gravitational constant, $m/s^2$
$h_i, h_f$	Initial and critical film thickness, m

$H(x, t)$	Population balance equation source term
$H$	Dispersion band thickness (or dispersion height in batch settler), m
$H_b$	Baffle opening height, cm
$H_t$	Height of the end-plate, cm
$k$	Turbulent kinetic energy per unit mass, $m^2/s^2$
$L$	Settling length, m
$L_i$	$i^{\text{th}}$ abscissa, m
$\langle l_w \rangle$	Average distance between bubbles, m
$l_e$	Integral length scale of turbulence, m
$m_k$	$k^{\text{th}}$ moment of bubble size distribution
$\vec{M}$	Interphase momentum exchange term, $kg/m^3 \cdot s$
$N$	Number of phases, (-)
$P$	Pressure, $N/m^2$
$p$	Drag correction factor, (-)
$P(v/v')$	Breakage probability term, $m^{-3}$
$P_c$	Coalescence efficiency
$r, r_1, r_2$	Bubble radius, m
$R_a$	Film radius, m
$s$	Source term due to coalescence and breakage
$Q$	Flow rate, l/hr
$Q_t$	Total flow rate, l/hr
$Q_d$	Disperse phase flow rate, l/hr
$Re$	Reynolds number, (-)
$t$	Time, s

$t_r$	Residence time, s
$u_{r1}, u_{r2}$	Terminal rise velocity of bubbles, $\text{ms}^{-1}$
$u_{rel}$	Relative velocity between bubbles, $\text{ms}^{-1}$
$U$	Phase velocity, m/s
$V_t$	Settling velocity, m/s
$V_I^{BOX}$	Volume influenced by a wake $\text{m}^3$
$V, V_1, V_2$	Bubble volume $\text{m}^3$
$w_i$	$i^{\text{th}}$ weight, (-)
$x$	Internal variables, $\text{m}^3$
$x, y, z$	Spatial coordinates (along width, height and depth, respectively), m
$v$	Velocity of particle, $\text{m}^3$

## Greek Letters

$\alpha$	Dispersed phase hold-up/volume fraction, (-)
$\beta$	Continuous phase hold-up/volume fraction, (-)
$\varepsilon$	Energy dissipation rate, $\text{m}^2/\text{s}^3$
$\mu$	Viscosity, $\text{kg}/\text{m}\cdot\text{s}$
$\mu_{eff}$	Effective viscosity, $\text{kg}/\text{m}\cdot\text{s}$
$\nu$	Kinematic turbulent viscosity, $\text{m}^2/\text{s}$
$\rho$	Density, $\text{kg}/\text{m}^3$
$\sigma$	Interfacial tension, $\text{mN}/\text{m}$
$\tau$	Stress tensor, Pa
$\Gamma(x', x-x')$	Coalescence kernels, (-)
$Y_i$	Fraction reassigned to nearby classes pivot, (-)

$\xi_{12}$	$r_1/r_2$
$\eta$	Test function, (-)

### **Superscripts**

$D, VM, L$	Drag, virtual mass and lift force, respectively
$c, b$	Continuous phase
$d, a$	Dispersed phase

### **Subscripts**

$G \text{ or } L$	Gas or liquid phase
$i$	Interface
$k$	Reference to phase k
$lam, t, eff$	Laminar, turbulent, effective